# In-situ Measurements of Magnetic Properties in Vacuum-Deposited Permalloy Films

**Abstract:** The quasi-static magnetic properties of vacuum-deposited Permalloy films of zero-magnetostrictive composition are examined *in situ* in an evaporator equipped with a laser-operated Kerr magneto-optic hysteresigraph. The coercive force, which depends strongly upon the film thickness, is large ( $H_c > 20$  Oe) when the hysteresis loop is first observable with a thickness of  $\sim 50$  Å for low substrate temperatures (T < 50°C) and  $\sim 100$  Å for high substrate temperatures (T > 100°C). There are two peaks of coercivity, at  $\sim 400$  Å and  $\sim 1,000$  Å; the two are thought to be related, respectively, to the transitions from the Néel to the cross-tie walls, and from the cross-tie to the Bloch walls. Two distinct components of the uniaxial anisotropy is induced; and  $K_2$ , which is readily re-oriented (with time constant less than 10 sec) along any angle between the easy and the hard axis. The net anisotropy field and the easy-axis orientation, both of which are affected by the  $K_2$  components, can be calculated for a given set of fabrication parameters. Experimental results agree well with the calculated values. The angular dispersion does not appear to be affected by the amplitude of the orienting field H or the nature of the field (a.c. or d.c.) when  $H > H_c$ . There is a slight increase in angular dispersion as the  $K_2$  component of the anisotropy rotates from the easy to the hard axis.

#### Introduction

During the past decade it has been conventional practice to prepare thin Permalloy films by vacuum deposition at an elevated substrate temperature but then to examine them at room temperature and atmospheric pressure.1 Magnetic properties measured in this way differ considerably among various workers, with the major discrepancy having to do with the coercive force  $H_c$  (usually measured on films of graded thickness on a large substrate) and with its dependence upon the film thickness.<sup>2-4</sup> There are a number of reasons for discrepancies, among which are the differences in film purity that are brought about by varying degrees of vacuum, and differences among starting materials, crucibles, and heating methods. Another, one that may be more significant, is non-uniformity of properties over the large area in which films of graded thicknesses are prepared.

As other discrepancies, we have that the magnitude and thickness dependence of the angular dispersion,  $\alpha_{90}$ , do not agree among workers.<sup>5,6</sup> Further, we have that the uniaxial anisotropy when subjected to an annealing operation has been reported<sup>7</sup> to reorient very rapidly in

fresh samples (in less than a few seconds), whereas airexposed films have been reported<sup>8</sup> to have a time constant of reorientation that exceeds one hour.

These results have suggested the desirability of *in-situ* examination of film properties during and after film preparation, for such would obviate contamination and allow a continuous measurement as a function of thickness. Webley<sup>9</sup> and more recently Lykken and Mitchell<sup>10</sup> performed an *in-situ* examination of static magnetic properties using an inductive-pickup hysteresigraph. The inherently poor sensitivity of such instrumentation did not permit accurate measurements on thin samples (<200 Å).

The purpose of our study, therefore, has been to examine the magnetic properties—in particular, the coercive force, the anisotropy, and the angular dispersion—obtaining in zero-magnetostrictive Permalloy films during and after preparation in a special evaporator equipped with a Kerr magneto-optic hysteresigraph. This consistent environment allows continuous and accurate measurements on a fixed spot ( $\sim$ 1/8-in. diam.) throughout the evaporation period and beyond.

477

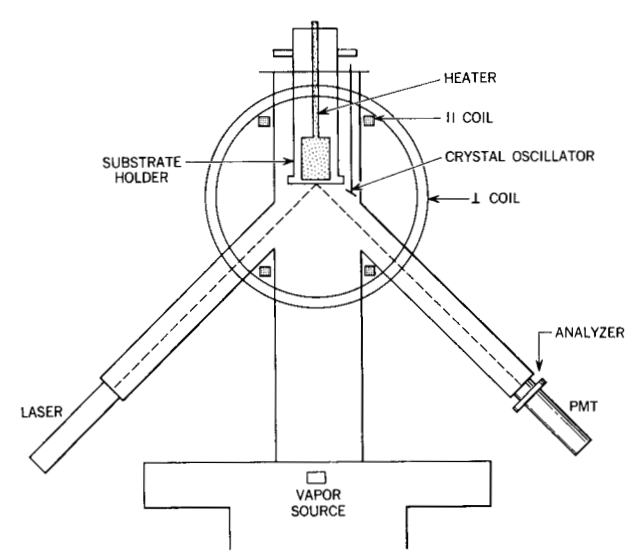


Figure 1. Arrangement of the evaporator-monitor system.

## **Experimental technique**

The basic components of the evaporator-monitor system are as illustrated in Fig. 1: (1) an inverted "double-Y" Pyrex chamber on which are mounted an analyzer, a photomultiplier tube, two orthogonal pairs of coils, a cw laser (1/2 mW at  $\lambda = 6328$  Å), and an interference filter with maximum transmission at  $\lambda = 6300$  Å; and (2) the vacuum system (with an oil diffusion pump) with two vapor sources.

The substrate holder, made of a copper block, could be operated from -196 °C to +500 °C, with provision for fast cooling with water (from 500°C to 100°C in less than 20 sec) and fast heating (from -196°C to 400°C in less than 10 min) with a massive copper block pre-heated to  $\sim 700$  °C. Highly polished semiconductor-grade silicon wafers (diameter: 1 in.; thickness: 0.008 in.) with a thermally grown SiO<sub>2</sub> film ( $\sim$ 5,000 Å) were selected to ensure uniformity of the substrate surface. (The roughness of the substrate as examined with an electron microscope by surface replication is illustrated in figures accompanying Appendix 1). The substrate was located ~40 cm above the vapor source (diameter: 1.6 cm). Films were evaporated at a rate of 3 to 6 Å/sec from a recrystallized alumina crucible placed in a Mo receptor (kept at positive potential) and bombarded by electrons from a tungsten filament (heated by a controlled direct current to minimize the extraneous signals picked up by the photomultiplier tube). Typical impurity contents in a melt, in a crucible, and in an evaporated film are listed in Table 1. The thickness of the film was monitored by a 4 MHz quartz crystal oscillator with a calibration constant of  $\sim 3$  Hz/Å. The pressure

Table 1a: Impurity contents in melt as examined by solid state mass spectrometer. Values in parentheses are data supplied by vendor.

Impurities <sup>(a)</sup>	Parts per million (atomic)		
Mn	5,000 (700)		
Cr	20 <sup>(b)</sup> (10)		
S	20		
Co	10 (20)		
Cu	10 (10)		
Ti, V, Zn	<0.5		

<sup>(</sup>a) Al, Si, F not analyzed due to interference.

Table 1b: Gas content in melt.

Gases	Percent (by weight)		
$O_2$ $N_2$	0.005 0.0007		

Table 1c: Impurity contents in alumina crucible (data supplied by vendor)

Impurities	Percent by weight		
$Al_2O_3$	99.7		
MgO	0.05-0.1		
SiO <sub>2</sub>	0.05-0.1		
CaO	0.02-0.05		
Na <sub>2</sub> O	0.005-0.05		
$Fe_2O_3$	0.03		
$Ga_2O_3$	0.01		
TiO <sub>2</sub>	0.004		
MnO	0.001		
B <sub>2</sub> O <sub>3</sub> , CdO	< 0.001		
ZnO, CuO, Cr <sub>2</sub> O <sub>3</sub> , V <sub>2</sub> O <sub>5</sub>	< 0.0005		

**Table 1d:** Impurity contents in monitor films (>  $2\mu$  thick) deposited on high-purity Au wire.

Impurities	Parts per million (atomic)		
Mn	20-10,000		
Ca	1000		
Sn	300		
Mo	200		
Ag	100		
Cu	70		
Co	30		
Cr	30		

during evaporation ranged (approximately) from  $5 \times 10^{-6}$  to  $1 \times 10^{-6}$  mm Hg. The residual gas contents in the evaporator before and during a typical evaporation are shown in Appendix 1. The wall coercive force was continuously monitored during evaporation with a 60 Hz drive field of  $\sim 1.2 H_c$  except during the initial stage of film growth, at which time more than  $\sim 20$  Oe was applied.

<sup>(</sup>b) Cr content was not constant.

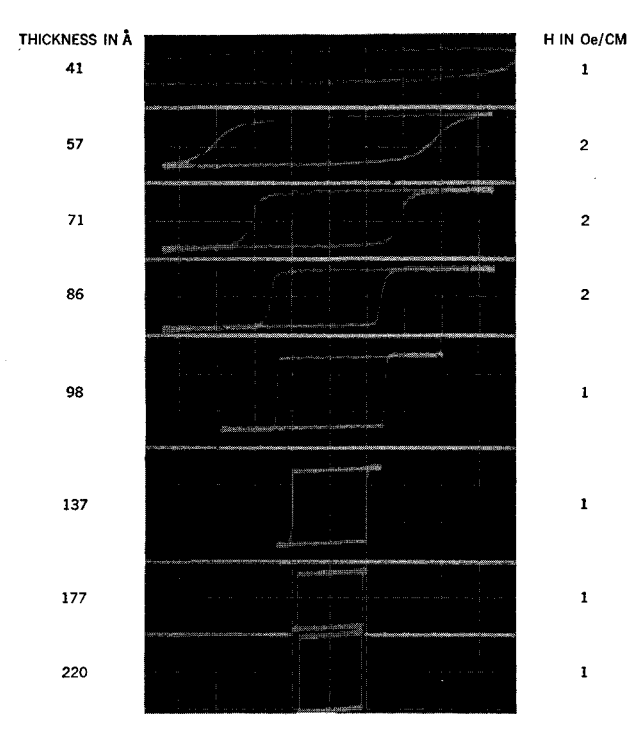


Figure 2. Hysteresis loops of Permalloy film observed during deposition at substrate temperature of 70°C. Thickness and *H*-scale calibration are as shown.

#### Coercive force

Since experimental results of the dependence of coercive force on film thickness and measurement temperature have been reported earlier, 11 we need but a summary here:

During the initial stage of film growth, the coercive force is large ( $H_c > 20$  Oe) and rounded hysteresis loops are evident when first observable at  $\sim 100$  Å at elevated substrate temperatures (T > 100 °C); it decreases rapidly, however, to  $H_c < 1$  Oe near 150 Å thickness, the loop meanwhile becoming square. In Figure 2 are shown hysteresis loops observed during a typical evaporation at a substrate temperature of 70 °C. The threshold thickness at which loops are observable appears to be related to the continuity of the film.

There is a strong dependence of  $H_c$  on thickness with two maxima, at  $\sim 400$  Å and  $\sim 1000$  Å, which are believed to be caused, respectively, by the transitions from Néel to cross-tie and transitions from cross-tie to Bloch domain wall structures. The dependence of  $H_c$  on measurement temperature (after film deposition) appears to be almost linear when T is less than  $T_{\rm deposition}$ . A typical rate of decrease of  $H_c$  with increasing temperature is 0.014 Oe/100°C. When the measurement temperature exceeds  $T_{\rm deposition}$  (T < 300°C) there occurs an irreversible increase in  $H_c$  which appears to be related to a structural change.

#### Anisotropy field

#### • Anisotropy spectrum

The macroscopic uniaxial anisotropy field may be separated into components, regardless of the mechanisms involved, by assuming that the film is composed of a single magnetic domain lying in the X-Y plane (Fig. 3) with the magnetization vector  $\mathbf{M}$  having constant magnitude M. The total energy per unit volume E under these conditions is given by:

$$E = -\mathbf{M} \cdot \mathbf{H} + K \sin^2 (\theta - \theta_0), \tag{1}$$

where  $\theta$  is the angle of **M**, and  $\theta_0$  is the direction of the easy axis (taken along the x-axis in the figure) with respect to arbitrary reference axes. The uniaxial anisotropy constant K may consist of several components in which case the last term may be replaced by:  $\sum_{i} K_{i} \sin^{2} (\theta - \beta_{i})$ . In practice (for example, as will be shown in Table 2) the total uniaxial anisotropy can be treated as composed of two distinct components:  $K_1$ , which is difficult to reorient (once the anisotropy is induced); and  $K_2$ , which is easily reoriented (by an applied field at an elevated temperature) with a much smaller time constant,  $\tau < 1$  sec. In freshly deposited films never exposed to air,  $K_2$  can be reoriented in less than a second at the deposition temperature by an applied field,  $H\gg H_k$ . In films exposed to air, a reorientation by the same amount requires, depending upon the annealing temperature relative to the deposition temperature, a much longer annealing period (typically, 60 minutes or more at deposition temperature). 8 In such a case, it is convenient to take  $\beta_1 = 0$  and  $\beta_2 = \beta$  (Fig. 3)

Figure 3. Angular relationship between magnetization M, applied field H, and anisotropy components  $K_1$  and  $K_2$ .

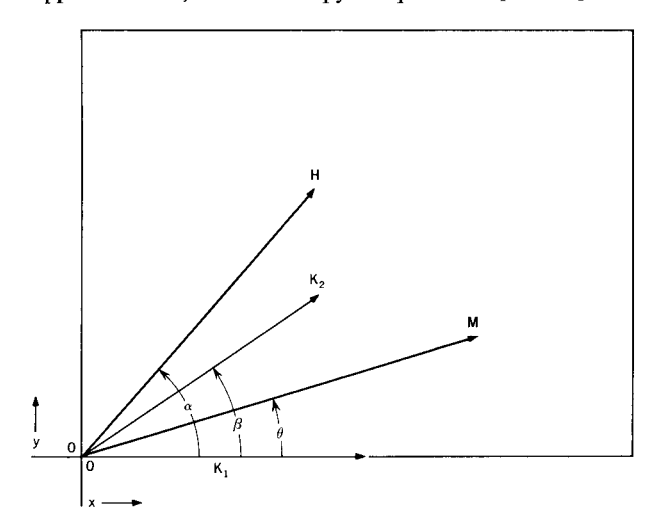


**Table 2** Comparison of  $H_k$  and  $\alpha_{00}$ , measured at room temperature, in films prepared under differing conditions. Film thickness: 1000 Å. Applied magnetic field (nominal): 20 Oe, a.c. or d.c.

Films	Magnetic Field		T	D	4 77	4
	Deposit <sup>(a)</sup>	Quench(a)	$T_{ m sub}$ (°C)	Range of $H_k$ (Oe)	Ave. $H_k$ (Oe)	Ave. $\alpha_{90}$ (deg)
Film A	a-c	a-c	275	4.0-4.5	4.2	1.7
Film B	d-c	d-c	275	4.0-4.2	4.1	1.5
Film C	d-c	d-c_l	275	2.0 - 2.4	2.3	2.5
Film D	d-c	d-c	175	4.6 - 4.8	4.7	2.2
Film E	d-c	a-c⊥	175	3.4-3.5	3.45	3.0

<sup>(</sup>a) Magnetic field applied during film deposition and quenching with a field parallel (||) or perpendicular (1) to the easy axis.

in which the total uniaxial anisotropy energy takes the form

$$E_a = K_1 \sin^2 \theta + K_2 \sin^2 (\theta - \beta)$$
  
=  $K \sin^2 (\theta - \theta_0)$ . (2)

Let us now consider the dependence of  $\theta$  on  $\beta$  for a given set of values  $K_1$  and  $K_2$ , which is characteristic of the film fabrication parameters. It is assumed that a large field  $H \gg H_{k_2}$  is applied to direction  $\beta$  so as to induce the  $K_2$  component along this direction.\* In the absence of a field the stable direction of M,  $\theta$ , is obtained at equilibrium:

$$\frac{\partial E_a}{\partial \theta} = K_1 \sin 2\theta + K_2 \sin 2(\theta - \beta) = 0.$$
 (3)

Thus, the dependence of  $\theta$  on  $\beta$  is given by

$$\operatorname{Tan} 2\theta = \frac{K_2 \sin 2\beta}{K_1 + K_2 \cos 2\beta}.$$
 (4)

Fig. 4 illustrates the angular relationships between  $K_1$ ,  $K_2$ , and K, which can also be derived from Eq. 2. From the figure, it is clear that

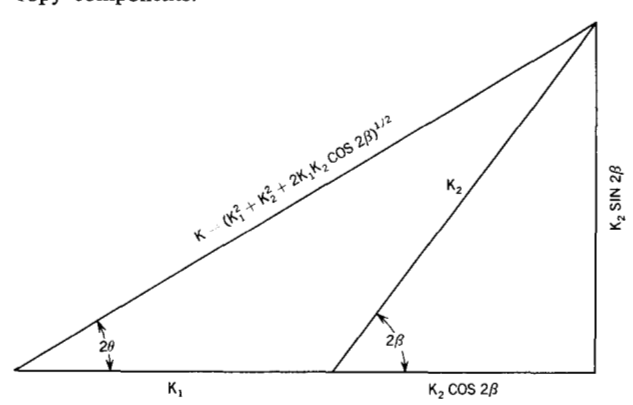
$$K = (K_1^2 + K_2^2 + 2K_1K_2\cos^2 2\beta)^{1/2}.$$
 (5)

The dependence on  $\beta$  of the stable angle  $\theta$  and the total anisotropy field  $H_k = 2K/M$  is shown in Fig. 5 for the two values k = 3.2 and 2.4 (where  $k = K_1/K_2$ ). The data of Fig. 5 are discussed below.

### • Results

The separation of K into  $K_1$  and  $K_2$  is easily achieved experimentally by inducing the  $K_2$  component along  $\theta = 0^{\circ}$  and 90° immediately after evaporation as shown in Table 2, where we have summarized essential data from Ref. 11. From Eq. 5,  $K = K_1 + K_2$  for  $\beta = 0^{\circ}$  and  $K = K_1 - K_2$  for  $\beta = 90^{\circ}$ . In Fig. 5 are shown experimental points of  $H_k$  and  $\theta$  for different values of  $\beta$  (for  $k = K_1/K_2 = 3.2$ ) together with calculated values. Although the scatter in the values of  $\theta$  appears large, it is reasonable

Figure 4. Relationship between angles  $\theta$  and  $\beta$  and anisotropy components.



<sup>\*</sup> Appendix 2 discusses the instance where this condition is not met.

in view of the ever-present skew of ~2° in normal evaporations. The values of the anisotropy field agree well with the calculated curve within the experimental error. The temperature-dependent properties of anisotropy fields are summarized in Fig. 6 together with comparable data from Smith<sup>7</sup> and data on bulk Permalloy (based upon Fe-pair ordering<sup>12</sup>). That the anisotropy field in films is increased over that of a bulk sample may well be due to fabrication parameters with, possibly, the most influential being the purity of the metal (usually less than 99.99%) and the effects of residual gases in the evaporator. Other candidates are the composition of crucible material, the heating methods, and the rate of evaporation. Since it is plausible that the admission of carbon pairs contributes to the total anisotropy, further work is warranted to identify possible origins and mechanisms of the uniaxial anisotropy. It should be fruitful to employ a more refined experimental technique, one combining a high-purity melt and, preferably, an ultra-high vacuum system (to minimize the hydrocarbons which may dissociate to hydrogen and carbon) equipped with an electron-beam source (to eliminate the crucible).

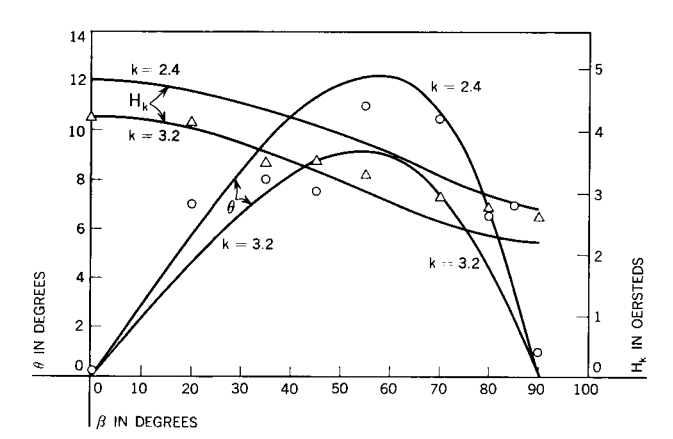


Figure 5. Dependence on  $\beta$  of total anisotropy field  $H_k$  and easy axis (stable angle  $\theta$ ). Calculated values are represented by solid lines; experimental points of  $H_k$  are represented by  $\triangle \ldots$  of  $\theta$  by  $\bigcirc$ .

#### Angular dispersion

The angular dispersion, which is a measure of the deviations of the local anisotropy from the macroscopic easy axis (of the whole film), was measured by Crowther's method.13 This dispersion does not appear to be affected by the magnitude of the applied field, in sharp contrast to data by Tolman and Oberg. 14 In many films which are prepared with an applied field less than  $1.5H_c$  (<1 Oe) e.g., the films shown in Fig. 3—the dispersion is between 1.5° and 2°. Thus, so long as the film is saturated along the easy axis due to an applied d-c field along the easy axis or pulsating between the two directions of the easy axis due to an applied a-c field, values of dispersion  $(\alpha_{90}) \sim 2^{\circ}$  are obtained. That the angular dispersion is not affected by the amplitude or the nature (a-c or d-c) of the orienting field suggests that the uniaxial anisotropy is induced by the magnetization M (M-induced anisotropy), to which exerts a much larger internal field on the newly forming layers on the substrate during evaporation than does the externally applied field. In films prepared for the anisotropy study, including those listed in Table 2, there is a slight increase in angular dispersion as the  $K_2$ component of the anisotropy rotates from the easy to hard axis, the maximum increase being less than 1°. This trend agrees well with the results of Tolman and Oberg<sup>14</sup> and Beam and Siegle.16

# Conclusions

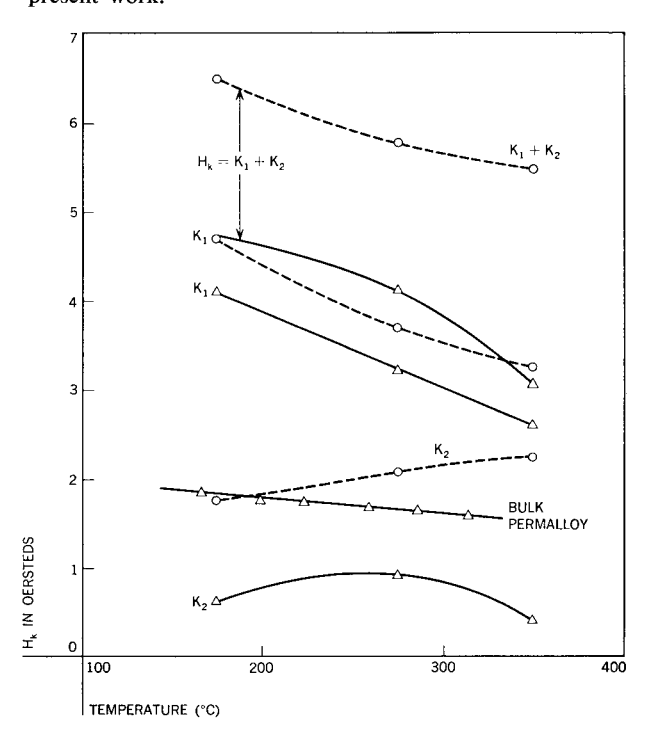
The quasi-static magnetic properties of Permalloy films of zero-magnetostrictive composition were examined in situ in a special evaporator equipped with a laser-operated Kerr magneto-optic hysteresigraph. The coercive force during the initial stage of film growth (with a thickness less than  $\sim 15 \text{ Å}$ ) is large ( $H_c \sim 10 \text{ Oe}$ ). This appears to

be related to the demagnetizing field as a result of the discontinuity of the film. In the thickness range of  $\sim 100$  Å to 2,000 Å, two peaks in  $H_c$  are observed (at  $\sim 400$  Å and  $\sim 1,000$  Å) which are thought to be related, respectively, to the transitions from the Néel to the cross-tie walls and from the cross-tie to the Bloch walls. The rate of decrease of  $H_c$  as a function of measurement temperature in films deposited at elevated temperatures (200 to 300°C) is  $\sim 0.14$  Oe/100°C. When, in films deposited below 400°C, the measurement temperature exceeds 400°C, an irreversible increase in  $H_c$  occurs, suggesting a sudden change in the structure of the film.

Two distinct components of anisotropy are identified:  $K_1$ , which is difficult to re-orient once the anisotropy is induced; and  $K_2$ , which can be easily rotated by an applied field at deposition temperature. Experimental values of the total anisotropy,  $H_k$ , and the direction of easy axis,  $\theta$ , agree well with calculated values as the  $K_2$  component rotates from  $\beta = 0^{\circ}$  to  $\beta = 90^{\circ}$ . Experimental values of  $K_1$  and  $K_2$  in Permalloy films are, respectively, found to be  $\sim$ 3.2 Oe and  $\sim$ 1 Oe for a deposition temperature of 275°C and, again respectively, to be  $\sim$ 4.1 Oe and  $\sim$ 0.6 Oe for a deposition temperature of 175°C.

The magnitude of the angular dispersion does not appear to be affected by the magnitude of the applied field so long as the applied field exceeds the coercive force. Moreover,

Figure 6. Dependence of anisotropy (measured at room temperature) with substrate temperature during deposition. Dashed lines are results from Ref. 7; solid lines are from the present work.



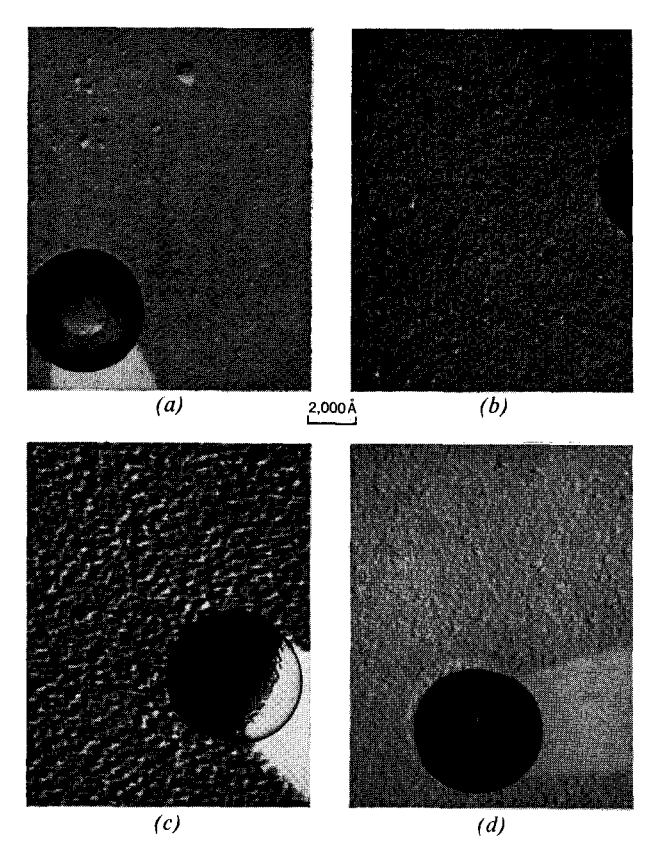


Figure A-1. Electron micrographs, as examined by surface replication technique, of four surfaces: (a) substrate; (b) Permalloy film (1000Å) deposited at 175°C; (c) Permalloy film (1000Å) deposited at 350°C; (d) Permalloy film (2000Å) deposited at -196°C and heated to 400°C. Diameter of the reference ball is 5000Å.

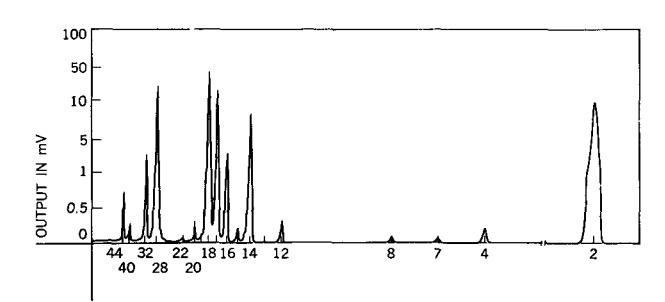


Figure A-2. Output signals from the residual gas analyzer as a function of mass-to-charge ratio *before* evaporation. Pressure  $= 1.5 \times 10^{-6}$  Torr; vertical scale  $= \times 30$  except for  $H_2$  where it is  $\times 300$ .

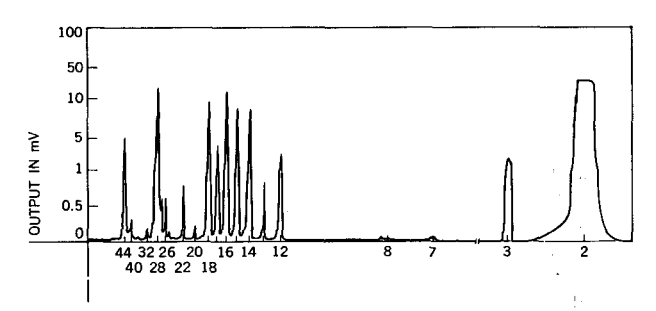


Figure A-3. Output signals from the residual gas analyzer as a function of mass-to-charge ratio *during* evaporation. Pressure  $= 3 \times 10^{-6}$  Torr; vertical scale  $= \times 30$  except for  $H_2$  where it is  $\times 300$ .

the nature of the applied field (a-c or d-c) does not seem to affect the angular dispersion. There is a slight increase in the magnitude of angular dispersion as the  $K_2$  component of the anisotropy rotates from the easy to hard axis with little variation in the product  $H_k\alpha_{90}$ . For example, in 250°C films the product decreases from 6.65 to 5.75 oersted degrees, while in 175°C films the product remains constant at 10.3 oersted degrees.

#### Appendix 1

In Figure A-1 we illustrate the typical surface roughness of the substrate as examined by an electron microscope using a surface replication technique and show Permalloy films deposited at different substrate temperatures. The average grain size of Permalloy films increases from  $\sim 100$  Å to  $\sim 200$  Å as the deposition temperature increases from  $-196\,^{\circ}$ C to  $+350\,^{\circ}$ C. Although not shown in the figure, there appears to be little variation in the microstructure of films deposited at  $-196\,^{\circ}$ C when subjected to high tem-

peratures for a brief period. Electron reflection diffraction studies on samples fabricated under similar conditions show that there is no preferred orientation in these polycrystalline films.

The mechanical stress in films prepared under similar conditions is of the order of  $10^9$  dyne/cm<sup>2</sup>. The adhesion of the films on substrate appears to be strong regardless of the deposition temperature; no peeling of the films was observed even when the low-temperature film was cycled between -196°C and +400°C.

The residual gas contents in the evaporator were analyzed before and during a typical evaporation (using a Veeco RG-4 Analyzer with a mass-to-charge ratio range of 2 to 50). The results are shown in Figs. A-2 and A-3. Gases that were predominant before evaporation are as given below, prefixed with their mass-to-charge ratios:

$$2(H_2^+)$$
,  $14(N_2^{++}, CH_2^+)$ ,  $16(O^+, CH_4^+)$ ,  $17(OH^+)$ ,  $18(H_2O^+)$ ,  $28(N_2^+, CO^+)$ ,  $32(O_2^+)$ , and  $44(C_3H_8^+)$ .

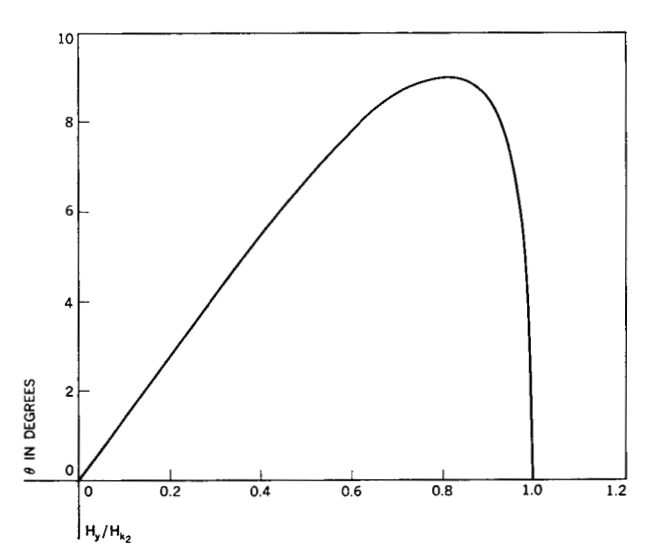


**Figure A-4.** Dependence of easy axis on H in a film with  $H_{k1} = 3.2$  Oe and  $H_{k2} = 1.0$  Oe.

The increase in pressure during evaporation appears to be caused mostly by the cracking of the pump-oil vapor (by electron beam), as indicated by sharp increases in hydro-carbon peaks with mass-to-charge ratios as follows:

$$2(H_2^+)$$
,  $12(C^+)$ ,  $13(CH^+)$ ,  $15(CH_3^+)$ ,  $16(CH_4^+)$ , and  $44(C_3H_3^+)$ .

#### Appendix 2

When the applied field H is small ( $H \cong H_k$ ), the direction of the induced  $K_2$  component is no longer parallel to that of H. Thus, one cannot substitute  $\beta$  into Eqs. (6) and (7). Instead, one needs to calculate values of  $\beta$  from Eq. 3

for given  $H_x$  and  $H_y$  (components of H along the x- and y-axis, respectively). The calculated values of the resultant easy axis  $\theta$ , as a function of applied field along the hard axis  $H_y$ , are plotted in Fig. A-4. For hard-axis annealing with a pulsating field, one could predict the resultant skew (as shown above) by using an equivalent d-c field.

#### **Acknowledgments**

The author is grateful to J. C. Slonczewski for technical discussions and to A. S. Nowick for perceptive criticisms. The technical assistance of J. M. Viggiano throughout the work must also be acknowledged.

#### References

- For example, M. Prutton, Thin Ferromagnetic Films, Butterworths, London, 1964.
- K. H. Behrndt and F. S. Maddocks, J. Appl. Phys. 30, 276S (1959).
- 3. C. O. Tiller and C. W. Clark, Phys. Rev. 110, 583 (1958).
- 4. S. Middelhoek, Thesis, U. of Amsterdam, 1961, p. 139.
- 5. H. Clow, Nature 191, 996 (1961).
- 6. K. D. Lever, Nature 196, 158 (1962).
- 7. D. O. Smith and G. P. Weiss, J. Appl. Phys. 36, 962 (1965).
- 8. W. T. Siegle and W. R. Beam, J. Appl. Phys. 36, 1721 (1965).
- 9. R. S. Webley, Nature 183, 999 (1959).
- G. I. Lykken and E. N. Mitchell, J. Appl. Phys. 36, 974 (1965).
- 11. K. Y. Ahn, J. Appl. Phys. 37, 1481 (1966).
- 12. S. Chikazumi, J. Phys. Soc. Japan 5, 333 (1960).
- 13. T. S. Crowther, M.I.T. Lincoln Laboratories Group Report 51-2, 1959.
- 14. C. H. Tolman and P. E. Oberg, 1963 Proc. INTERMAG Conference, April 1963, Washington, D. C., p. 13-31.
- 15. D. O. Smith, J. Appl. Phys. 32, 70S (1961).
- W. R. Beam and W. T. Siegle, 1964 Proc. INTERMAG Conference, April 1964, Washington, D. C., p. 9-3-1.

Received April 11, 1966